JOURNAL OF Materials CHEMISTRY

A theoretical study of atom ordering in copper–gold nanoalloy clusters

Nicholas T. Wilson and Roy L. Johnston*

School of Chemical Sciences, University of Birmingham, Edgbaston, Birmingham, UK B15 2TT. E-mail: roy@tc.bham.ac.uk; Fax: +44 (0)121 414 4403

Received 29th April 2002, Accepted 18th June 2002
First published as an Advance Article on the web 7th August 2002

Energy calculations have been carried out on high symmetry icosahedral and cuboctahedral Cu–Au nanoalloy clusters of various compositions, with the interatomic interactions modelled by the Gupta many-body potential. For each composition, the lowest energy isomers (''homotops'') tend to have predominantly Au atoms on the surface and Cu atoms in the core, and this phenomenon is explained in terms of surface energy, atomic size and trends in cohesive energies. A number of order parameters and mixing energies have been introduced and it is shown that there is good correlation between the cluster binding energy and the average distance of the Au atoms from the centre of the cluster. Comparisons are made with previous theoretical calculations on Cu–Au clusters, as well as with experimental studies of the structures and atom ordering of deposited Cu–Au particles.

1 Introduction

Clusters are aggregates of between a few and many millions of atoms or molecules. They may consist of identical atoms, or molecules, or two or more different species. Clusters are formed by most of the elements in the Periodic Table and can be studied in a number of media, such as molecular beams, the vapour phase, in colloidal suspensions and isolated in inert matrices or on surfaces.[1] Interest in clusters arises, in part, because they constitute a new type of material which may have properties which are distinct from those of discrete molecules or bulk matter, and also because their properties often vary significantly as a function of size.[1–3] In this paper, we present a theoretical study of the binding energies, mixing energies and ordering in high symmetry mixed copper–gold clusters (''nanoalloys'') with up to several hundred atoms. Such studies are important in increasing our understanding of how the structures, stabilities and atomic ordering of these clusters vary as a function of their size and composition, which will ultimately aid the design of nanomaterials with tailored physical and chemical properties.

1.1 Nanoalloy clusters

The range of properties of metallic systems can be greatly extended by taking mixtures of elements to generate intermetallic compounds and alloys.[4] In many cases, there is an enhancement in specific properties upon alloying, due to synergistic effects, and the rich diversity of compositions, structures and properties of metallic alloys has led to widespread applications in electronics, engineering and catalysis.

The desire to fabricate materials with well-defined, controllable properties and structures, on the nanometre scale, coupled with the flexibility afforded by intermetallic materials, has generated interest in bimetallic alloy clusters, or ''nanoalloys''. Such clusters have been studied in colloidal solutions, in the solid state, on solid supports and in molecular beams.[5–9]

One of the major reasons for the interest in nanoalloy particles is the fact that their chemical and physical properties may be tuned by varying the composition and atomic ordering, as well as the size of the clusters. Their surface structures, compositions and segregation properties[10] are of interest as they are important in determining chemical reactivity, and especially catalytic activity.[11,12] Nanoalloy clusters are also of interest as they may display structures and properties which are distinct from those of the pure elemental clusters. There are also examples of pairs of elements (such as Fe and Ag) which are immiscible in the bulk phase but which readily mix in finite clusters.[13]

A number of theoretical studies, mainly using empirical many-body potentials,[14] have been performed on intermetallic clusters.[8,9,15–20] Calculations based on semi-empirical molecular orbital methods and density functional theory (DFT) have also been applied to the study of bimetallic clusters.[21,22] Although these calculations have so far been limited to smaller clusters (with up to around 20 metal atoms), developments in computer hardware and algorithms should enable the study of larger clusters in the future. It should be noted that DFT calculations have previously been applied to monometallic clusters with as many as 147 atoms, where the larger clusters have high symmetry,[23] hence, there is scope for extending such studies to bimetallic clusters with tens or even hundreds of atoms. One possible way forward would be to use empirical potentials to guide the DFT calculations towards likely candidate structures.[24] This approach has been used by Catlow and co-workers to propose a structure for a mixed ruthenium–copper cluster with 16 metal atoms, formed by thermal decomposition of an organometallic precursor cluster within mesoporous silica.[22]

1.2 Homotops

On going from pure metal clusters to bimetallic nanoalloys, there is an increase in complexity, due to the presence of two different types of atoms, which leads to the possibility of isomers based on the permutation of unlike atoms, as well as the regular geometrical isomers (with different skeletal structures). Jellinek and co-workers have introduced the term ''homotops'' to describe A_aB_b alloy cluster isomers, with a fixed number of atoms ($N = a + b$) and composition (a/b ratio), which have the same geometrical arrangement of atoms, but differ in the way in which the A and B-type atoms are arranged.[9,17–20]

As the number of homotops rises combinatorially with cluster size, global optimisation (in terms of both geometrical isomers and homotops) is an extremely difficult task. Ignoring point group symmetry, a single geometrical isomer of an N-atom AB cluster will give rise to ${}^{N}P_{A,B}$ homotops (eqn. 1),

$$^{N}P_{A,B} = \frac{N!}{N_A!N_B!} = \frac{N!}{N_A!(N-N_A)!} \quad (1)$$

where N is the total number of atoms, N_A is the number of atoms of type A and N_B is the number of atoms of type B. For a 20-atom $A_{10}B_{10}$ cluster, for example, there are 184756 homotops, though many may be symmetry-equivalent. The total number of homotops of any composition for a given structural isomer is 2^N, which is approximately 10^6 for a 20-atom cluster.

In this work, as well as geometrical isomers and homotops, we shall also use the term "composomers"[25] to refer to compositional isomers, *i.e.* nanoalloy clusters with the same number of atoms ($N = N_A + N_B$) and geometrical (skeletal) structure, but with different compositions (N_A/N_B).

1.3 Cu–Au nanoalloy clusters

The "noble metals", copper, silver and gold, occur naturally as the free metals, but they invariably have trace amounts of other noble metals incorporated into their lattices. Their similar electronegativities and $d^{10}s^1$ electronic structures facilitate the alloying of these elements in the solid state.[4] In addition to the extensive research on bulk alloy Cu–Au phases, in recent years, there have been a number of experimental and theoretical studies of Cu–Au nanoalloys.

In the early 1990s, Mori and co-workers used transmission electron microscopy (TEM) to study the dissolution of copper atoms in nanometre-sized gold clusters.[6,26] Yasuda and Mori subsequently studied stoichiometric $(Cu_3Au)_M$ clusters, which were prepared by dual-source vaporisation using an electron beam.[27] Copper–gold nanoalloy clusters have also been generated by Lievens and co-workers by using a dual-laser vaporisation source (to produce Cu–Au clusters of varying compositions) and by laser vaporisation of bulk alloy (CuAu, Cu_3Au and $CuAu_3$) targets.[7,8] In the later experiments, the Cu–Au clusters were deposited on amorphous carbon and MgO substrates.[8] The results of these experiments will be discussed later.

Compared to pure copper and gold clusters, Cu–Au nanoalloy clusters have not been as thoroughly investigated from a theoretical viewpoint, due to the additional difficulty of considering the hetero-, as well as the homometallic interactions, and the occurrence of a large number of homotops. López *et al.* have made a detailed study of 13- and 14-atom nanoalloy clusters, Cu_xAu_y, of various compositions.[16] For the different atom combinations, they found that all of the clusters, except the pure Au_{14} cluster, have icosahedral-type geometries, while the Au_{14} cluster has a distorted hexagonal antiprismatic structure, with C_{6v} symmetry.

The importance of homotops can be appreciated by considering the hierarchy of isomers of Cu_6Au_7, for which López *et al.* found the first 15 lowest energy isomers to be homotops, with the same geometrical structure.[16] They concluded (based on the melting transitions of the icosahedral structures) that the bimetallic clusters resemble copper clusters more closely than gold ones—dynamically as well as structurally. Gold clusters, for example, only exhibit a single stage of melting, whereas pure copper and alloy clusters display two stages. Other recent theoretical studies of Cu–Au nanoalloys will be discussed below.

1.4 Geometric shells and subshells

In this study, in order to cut down on computational expense, we have focussed on high symmetry icosahedral and cuboctahedral "geometric shell" clusters[28,29] (composed of centred, concentric polyhedral shells) with up to several hundreds of atoms. Icosahedral and cuboctahedral structures are commonly observed for elemental metal clusters.[1] The icosahedron is an example of a non-crystalline packing (the 5-fold symmetry axes of the icosahedron are incompatible with 3-D translational symmetry), while the cuboctahedron has an fcc arrangement of atoms, as in the stoichiometric ordered Cu–Au phases CuAu, Cu_3Au and $CuAu_3$.[3]

Table 1 Number of atoms in the k^{th} shell [$S(k)$] and total number of atoms in a k-shell cluster [$N(k)$] for 1–5-shell icosahedral and cuboctahedral clusters

k	1	2	3	4	5
$S(k)$	12	42	92	162	252
$N(k)$	13	55	147	309	561

Because icosahedral and cuboctahedral clusters are both based on 12-vertex polyhedra, closed geometric shell icosahedral and cuboctahedral clusters have the same numbers of atoms. The number of atoms in the k^{th}shell, $S(k)$, and the total number of atoms (including the central atom), $N(k)$, of an icosahedral or cuboctahedral geometric shell cluster are given by eqn. 2 and 3, respectively.

$$S(k) = 10k^2 + 2 \quad (2)$$

$$N(k) = \frac{1}{3}(10k^3 + 15k^2 + 11k + 3) \quad (3)$$

$S(k)$ and $N(k)$ values are listed in Table 1 for icosahedral/cuboctahedral clusters with 1–5 shells. A cross-section through a 5-shell (561-atom) icosahedral cluster is shown in Fig. 1, where the different shells of atoms are represented by different colours.[31]

To calculate the energies of all possible homotops for nanoalloy clusters with several hundred atoms would be computationally infeasible, so in this study we have considered only those homotops where all the atoms forming a symmetry-equivalent set (*i.e.* a geometric "subshell"[28,29]) are constrained to be of the same element. This has the advantages of reducing the number of isomers to a manageable level and maintaining the symmetry of the cluster, leading to greater efficiency in the calculation of the potential energy. Fig. 2 shows the subshells of the outermost shell of a 5-shell (561-atom) icosahedral cluster, with the different subshells being indicated by different colours.

The number of atoms in each subshell are listed in Table 2 for icosahedral (ico) and cuboctahedral (cub) clusters with 1–5 shells.[31] Within each shell, the subshells are listed in order of increasing distance from the centre of the cluster. The different types of subshells are labelled according to which topological sites the atoms occupy in the cluster polyhedron: v = vertex; e = edge; f = face.

A convenient way of defining the high symmetry homotops (with all atoms in each subshell being of the same type) is as a

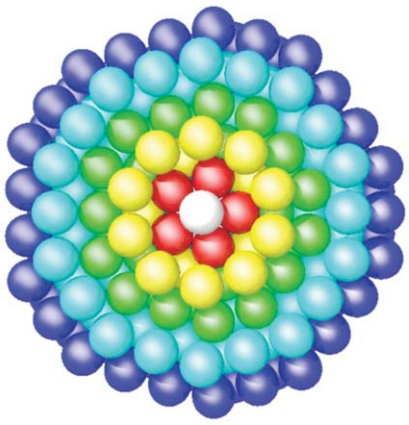

Fig. 1 Cross-sectional view of a 5-shell icosahedral cluster showing the shell structure (indicated by different colours).

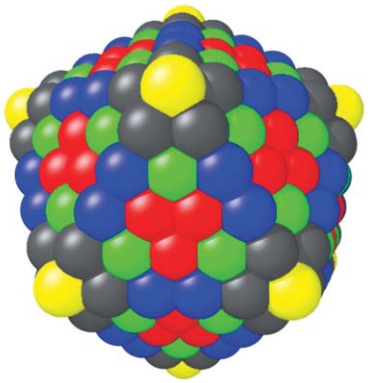

Fig. 2 Subshells (indicated by different colours) in the outer shell of a 5-shell (561-atom) icosahedral cluster.

string of atomic labels (in the present case "Au" and "Cu") indicating the atom type of each subshell, where the subshells are ordered as in Table 2. For a 5-shell icosahedral cluster, the ordering is therefore: {0c 1v 2e 2v 3f 3e 3v 4f 4e 4e 4v 5f 5f 5e 5e 5v}, where the number is the index of the shell (using 0 to represent the centre of the cluster), c denotes the central atom and v, e and f denote vertex-, edge- and face-localised atoms, respectively, as in Table 2. The string {Au Cu Cu Au}, for example, identifies a 55-atom icosahedron with a central gold atom, copper atoms in the first shell and on the edges of the second shell and gold atoms on the vertices of the second shell.

Finally, it should be noted that, as we have constrained all atoms in each icosahedral or cuboctahedral subshell to be of the same type, none of the nanoalloy clusters (even the fcc-like cuboctahedral clusters) that we have studied have the observed atomic ordering and stoichiometries of the ordered bulk phases CuAu, Cu_3Au or $CuAu_3$. (Cuboctahedral clusters based on these ordered arangements of atoms generally have tetragonal (D_{4h}), rather than cubic (O_h) symmetries.) Studies on Ni–Al clusters, including cuboctahedral clusters which were generated as fragments of the bulk ordered Ni_3Al and NiAl phases,[32] have shown that this is likely to lead to very little change in the cluster binding energy compared to the most stable high symmetry (I_h or O_h) clusters studied here.

2 Computational details

2.1 The Gupta potential

Since, for large clusters (of hundreds or thousands of atoms), *ab initio* calculations are still, at present, infeasible, there has been much interest in developing empirical atomistic potentials for the simulation of such species. In this work, we have adopted the empirical Gupta many-body potential.[33] Empirical potentials, such as the Gupta potential,[33] are derived by fitting experimental data to an assumed functional form. The Gupta potential has been derived from Gupta's expression for the cohesive energy of a bulk material[34] and can be written in terms of repulsive pair (V^r) and attractive many-body (V^m) terms, which are obtained by summing over all (N) atoms:

$$V_{clus} = \sum_{i}^{N} \{V^r(i) - V^m(i)\} \quad (4)$$

where

$$V^r(i) = \sum_{j}^{N}{}' A(a,b) \exp\left(-p(a,b)\left(\frac{r_{ij}}{r_0(a,b)} - 1\right)\right) \quad (5)$$

and

$$V^m(i) = \left[\sum_{j}^{N}{}' \zeta^2(a,b) \exp\left(-2q(a,b)\left(\frac{r_{ij}}{r_0(a,b)} - 1\right)\right)\right]^{\frac{1}{2}} \quad (6)$$

In eqn. 4 and 5, r_{ij} is the distance between atoms i and j in the cluster and A, r_0, ζ, p and q are fitted to experimental values of the cohesive energy, lattice parameters and independent elastic constants for the reference crystal structure at 0 K. The primes indicate summation over all atoms j, except $j = i$.

For Cu_xAu_y alloy clusters, the parameters take different values for each of the different types (Cu–Cu, Cu–Au and Au–Au) of interaction. In the above equations, a and b are the atom labels for atoms i and j, respectively. The homonuclear (Cu–Cu and Au–Au) parameters were derived by fitting to the pure metals and are taken to be unchanged in the alloys. The heteronuclear (Cu–Au) parameters were obtained by fitting to crystalline Cu_3Au. The Gupta parameters used in this study, which were derived by Cleri and Rosato,[33] are listed in Table 3.

It should be noted that the most stable crystalline structures for Cu, Au and the three alloy compositions studied correspond to fcc packing of atoms. In terms of the arrangement of the Cu and Au atoms, the bulk alloys Cu_3Au and $CuAu_3$ have cubic symmetry ($L1_2$), while CuAu has a layered tetragonal structure ($L1_0$).[4]

From the total cluster potential energy, V_{clus}, the average binding energy for an N-atom cluster is defined as the positive quantity:

$$E_b = \frac{-V_{clus}}{N} \quad (7)$$

Table 3 Parameters defining the Gupta potential for Cu–Au clusters[33]

Parameter	Cu–Cu	Cu–Au	Au–Au
A/eV	0.0855	0.1539	0.2061
p	10.960	11.050	10.229
r_0/Å	2.556	2.556	2.884
ζ/eV	1.2240	1.5605	1.7900
q	2.2780	3.0475	4.0360

Table 2 The number of atoms in each subshell (and the subshell type: v = vertex; e = edge; f = face) for the k^{th} shell of 1–5-shell icosahedral (ico) and cuboctahedral (cub) clusters.

	k	Number of atoms in each subshell (subshell type)							
ico	1	12 (v)							
	2	30 (e)	12 (v)						
	3	20 (f)	60 (e)	12 (v)					
	4	60 (f)	30 (e)	60 (e)	12 (v)				
	5	60 (f)	60 (f)	60 (e)	60 (e)	12 (v)			
cub	1	12 (v)							
	2	6 (f)	24 (e)	12 (v)					
	3	24 (f)	8 (f)	48 (e)	12 (v)				
	4	6 (f)	24 (f)	24 (f)	24 (f)	24 (e)	48 (e)	12 (v)	
	5	24 (f)	24 (f)	48 (f)	24 (f)	24 (f)	48 (e)	48 (e)	12 (v)

2.2 Radial relaxation of icosahedral and cuboctahedral nanoalloys

As Cu–Cu and Au–Au bond lengths are different (which is manifested in the different r_0 parameters in the Gupta potential—see Table 3),[36] starting with a pure copper cluster and introducing gold atoms (or *vice versa*) can lead to strained structures, which must be relaxed (energy minimised). In this study, we have performed radial relaxations on all the compositional isomers and homotops of closed icosahedral geometric shells, where the atoms within each given subshell are either all Cu or all Au. This radial relaxation is accomplished by minimising the energy as a function of the radii of all of the subshells,[31] using the conjugate gradients NAG routine E04UCF.[37] For atoms which do not lie on rotation axes of symmetry, tangential relaxation (*i.e.* motion perpendicular to the radial vector) is also possible, though previous calculations have shown that such relaxations are small and lead to very small changes in cluster binding energy.[29]

As shown in Table 2, 1–5-shell icosahedral clusters possess 1, 3, 5, 10 and 15 subshells, respectively. A cluster with n subshells has 2^{n+1} subshell homotops (because the central atom effectively constitutes another subshell) and so 4, 16, 64, 2048 and 65536 radial minimisations are required for 1 to 5 shells, respectively. As the cuboctahedron has lower point group symmetry than the icosahedron (O_h instead of I_h), there are significantly more subshells in a cuboctahedral cluster than an icosahedral cluster of a similar size: 1–5-shell cuboctahedral clusters have 1, 4, 8, 15 and 23, subshells respectively. Because of this increase in the number of subshells, and hence in the number of homotops, it was decided to limit the present study to 1–4-shell cuboctahedral clusters, which were radially relaxed, as described above.

2.3 Order parameters

Order parameters assign a numerical value to a structural feature of a cluster, such as the degree of mixing. This aids the analysis of the large amounts of data generated by such a large number of isomers (both composomers and homotops) to determine the salient features which impart enhanced stability in these systems. A number of order parameters may be defined, some of which will be studied here.

The first order parameter that we have chosen to investigate is one based on the number of A–B nearest-neighbour interactions relative to the total number of nearest-neighbour interactions:

$$O_{\mathrm{nn}} = \frac{\sum_{i=1}^{N_{\mathrm{A}}} \sum_{j=N_{\mathrm{A}}+1}^{N} \delta_{ij}}{\sum_{i=1}^{N-1} \sum_{j=i+1}^{N} \delta_{ij}} \tag{8}$$

where

$$\delta_{ij} = \begin{cases} 1 & r_{ij} \leq 1.2 r_{\mathrm{nn}} \\ 0 & r_{ij} > 1.2 r_{\mathrm{nn}} \end{cases} \tag{9}$$

and r_{nn} is the nearest-neighbour distance within the cluster. The larger this value, the higher the degree of mixing in the cluster.

The average distance of an atom of type A from the centre of the cluster,

$$\langle R_{\mathrm{A}} \rangle = \frac{1}{N_{\mathrm{A}}} \sum_{i=1}^{N_{\mathrm{A}}} \sqrt{x_i^2 + y_i^2 + z_i^2} \tag{10}$$

can also be used as a measure of the degree of mixing within the cluster. A small $\langle R_{\mathrm{A}} \rangle$ value indicates a segregated cluster with the A atoms at the centre of the cluster, a medium value indicates a well-mixed cluster and a large value indicates a segregated cluster with the A atoms at the surface of the cluster. An alternative, related measure is the radius of gyration (the root mean square radius) of each subset of atoms, but this has not been considered here.

2.4 Mixing energies

The energy of mixing of the two components in a bulk alloy or nanoalloy cluster can also be used as a measure of order or disorder. Jellinek and Krissinel have defined the following mixing (potential) energy:[17]

$$V_{\mathrm{mix}} = V_{\mathrm{A}_n\mathrm{B}_m} - [V_{\mathrm{A}_n}^{(\mathrm{A}_n\mathrm{A}_m)} + V_{\mathrm{B}_m}^{(\mathrm{B}_n\mathrm{B}_m)}] \tag{11}$$

where $V_{\mathrm{A}_n\mathrm{B}_m}$ is the potential energy of the $\mathrm{A}_n\mathrm{B}_m$ cluster, $V_{\mathrm{A}_n}^{(\mathrm{A}_n\mathrm{A}_m)}$ is the binding energy of the A_n subcluster in the $\mathrm{A}_n\mathrm{A}_m$ cluster and $V_{\mathrm{B}_m}^{(\mathrm{B}_n\mathrm{B}_m)}$ is the binding energy of the B_m subcluster in the $\mathrm{B}_n\mathrm{B}_m$ cluster. These latter two terms are calculated by using the same atomic configuration, but with either all A or B atoms, partitioning the energy into contributions from each atom and counting only the contributions from the atoms in either the A_n or B_m subcluster. When comparing this value between isomers which have different potential energies the mixing coefficient:

$$M = \left(\frac{V}{V_{\mathrm{mix}}} \right) \times 100\% \tag{12}$$

is a more useful comparative tool. The mixing energy corresponds to the change in energy on constructing the alloy cluster from identical configurations of the elemental clusters. It involves interactions throughout the cluster, as opposed to the nearest-neighbour order parameter, which has a much smaller range.

When deriving parameters for bulk alloys, Cleri and Rosato[33] used the experimental enthalpy of mixing, ΔH_{mix}, as a parameter in the fitting of the potential, *via* the equation:

$$\Delta H_{\mathrm{mix}} = x_{\mathrm{A}} E_{\mathrm{c}}^{\mathrm{A}} + x_{\mathrm{B}} E_{\mathrm{c}}^{\mathrm{B}} - E_{\mathrm{c}}^{\mathrm{AB}} \tag{13}$$

where $E_{\mathrm{c}}^{\mathrm{AB}}$ is the cohesive energy of the bulk alloy system, $E_{\mathrm{c}}^{\mathrm{A}}$ and $E_{\mathrm{c}}^{\mathrm{B}}$ are the cohesive energies of the pure bulk elements and x_{A} and x_{B} ($= 1 - x_{\mathrm{A}}$) are the mole fractions of the elements A and B, respectively. In eqn. 13, it is assumed that the enthalpy of mixing is approximately the same as the internal energy change on mixing for solids. For the Cu_3Au bulk fcc solid, the mixing enthalpy has a small exothermic value of -2.07 kJ mol(atoms)$^{-1}$.[35]

In this study, we have considered a variation of eqn. 13, defining the change in cluster binding energy on mixing:

$$\Delta E_{\mathrm{mix}} = E_{\mathrm{b}}^{\mathrm{AB}} - F_{\mathrm{A}} E_{\mathrm{b}}^{\mathrm{A}} - F_{\mathrm{B}} E_{\mathrm{b}}^{\mathrm{B}} \tag{14}$$

where $E_{\mathrm{b}}^{\mathrm{AB}}$ is the binding energy (per atom) of the N-atom AB nanoalloy cluster, $E_{\mathrm{b}}^{\mathrm{A}}$ and $E_{\mathrm{b}}^{\mathrm{B}}$ are the cohesive energies of the pure A_N and B_N clusters and F_{A} and F_{B} ($= 1 - F_{\mathrm{A}}$) are the fractions of A and B atoms (eqn. 15) in the nanoalloy clusters.

$$F_{\mathrm{A}} = \frac{N_{\mathrm{A}}}{N} \tag{15}$$

A positive value of ΔE_{mix} corresponds to a nanoalloy cluster which is thermodynamically stable with respect to pure elemental clusters of the same size.

3 Results and discussion

3.1 Icosahedral nanoalloy clusters

The binding energies of all the radially-relaxed composomers and homotops for 1–5-shell icosahedral clusters are displayed in Fig. 3. The red points denote clusters where the surface shell is entirely composed of gold atoms. The green points denote clusters where the surface shell is completely copper. The blue points denote clusters where the shells at the core of the clusters

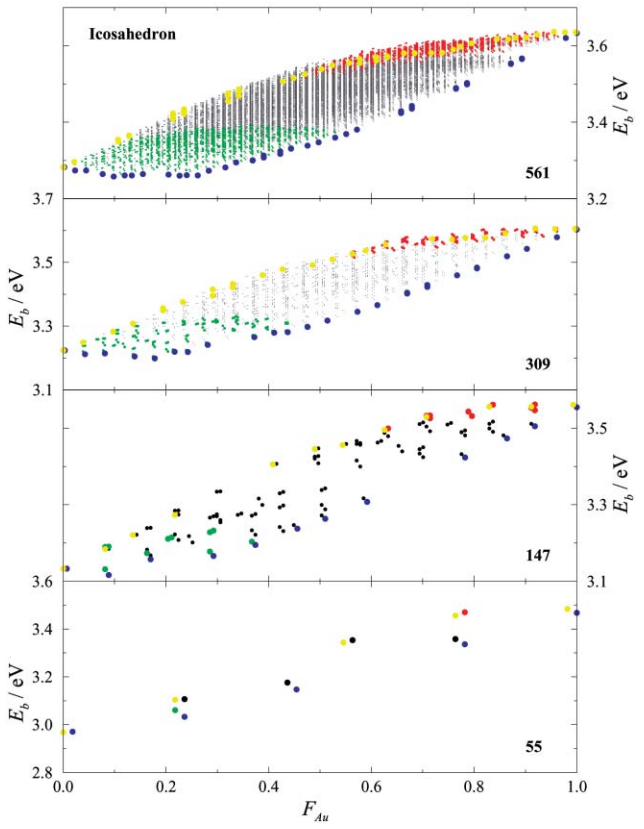

Fig. 3 Plot of binding energy (E_b) *vs.* the fraction of gold atoms (F_{Au}) for Cu_nAu_m icosahedral clusters, where $n + m$ is 55, 147, 309 and 561 atoms. Key: red = Au at surface; green = Cu at surface; blue = Cu surface and Au core; yellow = Au surface and Cu core.

are completely gold and those at the surface are completely copper. The clusters corresponding to the yellow points have the opposite arrangement. In these latter cases, the shell between the core and the surface can have a mixed composition. The black points correspond to other, more mixed arrangements. As the effect of mixing on the binding energy is small, there is not a pronounced maximum in the binding energy, due to strong exothermic mixing, though (as shown in Table 4) some copper inclusion is favoured. Generally, clusters with copper at the core and gold on the surface (red and yellow points in Fig. 3) are the most stable, which can be rationalised in terms of the lower surface energy of gold (96.8 meV $Å^{-2}$), as compared with copper (113.9 meV $Å^{-2}$),[42,43] as well as the minimisation of strain (see argument below). The unfavourable energy associated with placing Cu atoms on the surface and Au atoms in the core of the cluster can be appreciated from the low E_b values corresponding to the blue points in Fig. 3.

The lowest energy isomers of any composition for 1–5-shell icosahedral nanoalloys are listed in Table 4. The isomers are defined using the notation described above. As the binding energy within the pure gold clusters is larger than in the pure copper clusters and the enthalpy of mixing in the alloy system is small, the lowest energy clusters are predominantly composed of gold atoms, as has previously been observed for smaller Cu–Au clusters.[16,25,38] This is consistent with the order of cohesive energies of the bulk Cu–Au alloy phases [Au (3.81) > $CuAu_3$ (3.75) > CuAu (3.74) > Cu_3Au (3.64) > Cu (3.49 eV)],[35,36,39] and, in turn, is manifested in the values of the energy scaling parameters A and ζ, which follow the order (see Table 3): Au–Au > Cu–Au > Cu–Cu.

As the inner atoms in icosahedral clusters of single elements are usually under compression, so as to maximise surface atom interactions,[28,40,41] such clusters possess a destabilising bulk strain energy.[41] The smaller size of copper atoms (which is reflected in the shorter lengths of the Cu–Cu and Cu–Au bonds relative to the Au–Au bond, as shown in Table 3) allows this inherent strain to be partially relieved. In the 13- and 55-atom clusters, placing a Cu atom at the centre of the cluster allows the shorter radial distances in the cluster to be Cu–Au interactions and the longer tangential interactions to be Au–Au. For larger icosahedra, the most stable configurations place copper atoms in the vertex positions of the first or first and second shells. This does not alleviate the strain in the core of the cluster but has a marked effect on the strain in the outer shells, thus enhancing the stability of the system over the pure gold cluster.[38]

The mixing energies, ΔE_{mix} (eqn. 14), of the most stable clusters for each composition at each nuclearity are shown in Fig. 4 as a function of the fraction of gold atoms in the cluster, F_{Au}. The energies of the reference systems against which the

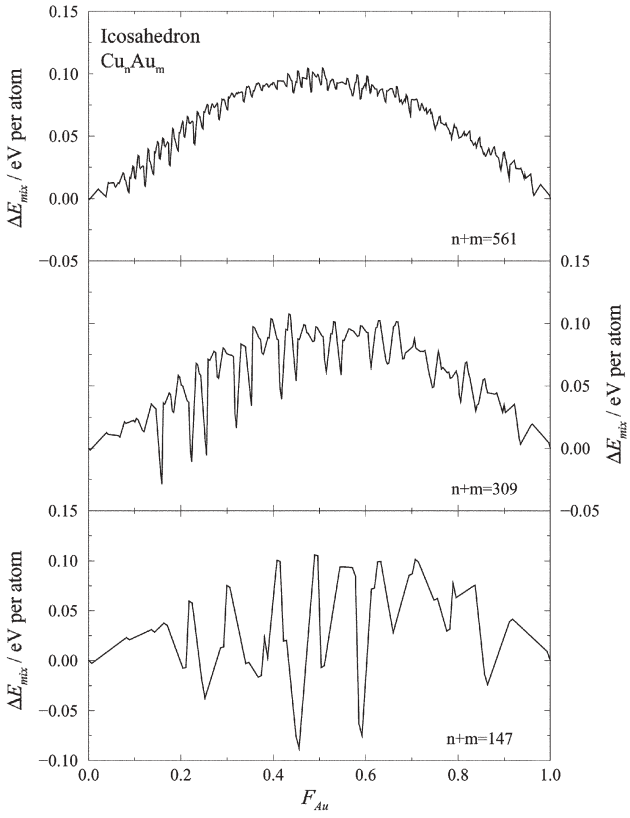

Fig. 4 Plot of mixing energy (ΔE_{mix}) *vs.* the fraction of gold atoms (F_{Au}) for 147-, 309- and 561-atom Cu–Au icosahedral clusters.

Table 4 The lowest energy icosahedral nanoalloy clusters with 1–5 closed geometric shells. In each case, the total number of atoms (N), the number of gold atoms (N_{Au}), the binding energy (E_b) and the subshell labelling are listed.

N	N_{Au}	E_b/eV	Subshell labelling
13	12	3.317736	{Cu Au}
55	54	3.483880	{Cu Au Au Au}
147	135	3.562092	{Au Cu Au Au Au Au Au}
309	285	3.608880	{Au Cu Au Cu Au Au Au Au Au Au Au}
561	537	3.638140	{Au Cu Au Cu Au Au Au Au Au Au Au Au Au Au Au Au}

mixing energies are calculated, E_b^A and E_b^B in eqn. 14, are the binding energies of the pure copper and gold icosahedra. The mixing energy is independent of cluster size and has a maximum value of 0.1 eV per atom for a 50 : 50 composition. That the maximum occurs at $F_{Au} = 0.5$, rather than 0.25 or 0.75, is consistent with the fact that, for the bulk alloy phases, ΔE_{mix} is greater for CuAu than for either Cu_3Au or $CuAu_3$ (where ΔE_{mix} now refers to the difference in bulk cohesive energies).[35,39] For small clusters, there are some negative ΔE_{mix} values, corresponding to composomers for which there is no homotop with a high binding energy. As the cluster size increases, however, a smoother positive trend is observed, corresponding to energy-favoured mixing. These results are consistent with the slightly exothermic experimental enthalpy of mixing in the bulk Cu_3Au system.[35]

The average distance of the gold atoms from the centre of the cluster, $\langle R_A \rangle$ in eqn. 9, and the nearest-neighbour order parameter, O_{nn} in eqn. 7, were calculated for all the homotops arising from four composomers of the 561-atom icosahedron. These compositions ($Cu_{309}Au_{252}$, $Cu_{308}Au_{253}$, $Cu_{253}Au_{308}$ and $Cu_{252}Au_{309}$) were chosen because they have similar numbers of Cu and Au atoms and have limiting segregated shell structure, arising from filling the outer shell (252 atoms) or the first four shells (308 atoms) with one type of atom, the central atom being either Cu or Au. $\langle R_{Au} \rangle$ and O_{nn} are plotted against the binding energy in Fig. 5 and 6, respectively.

Fig. 5 shows that the binding energy correlates well with the average distance of the gold atoms from the centre of the cluster ($\langle R_{Au} \rangle$), confirming that the lowest energy homotops have gold on the surface (as discussed above). The correlation of E_b with the nearest-neighbour order parameter (O_{nn}), however, is generally poor, as can be seen in Fig. 6. This is not surprising, since we have already seen that the most stable (highest E_b) clusters tend to have segregated structures rather than ordered, extensively mixed arrangements. However, there

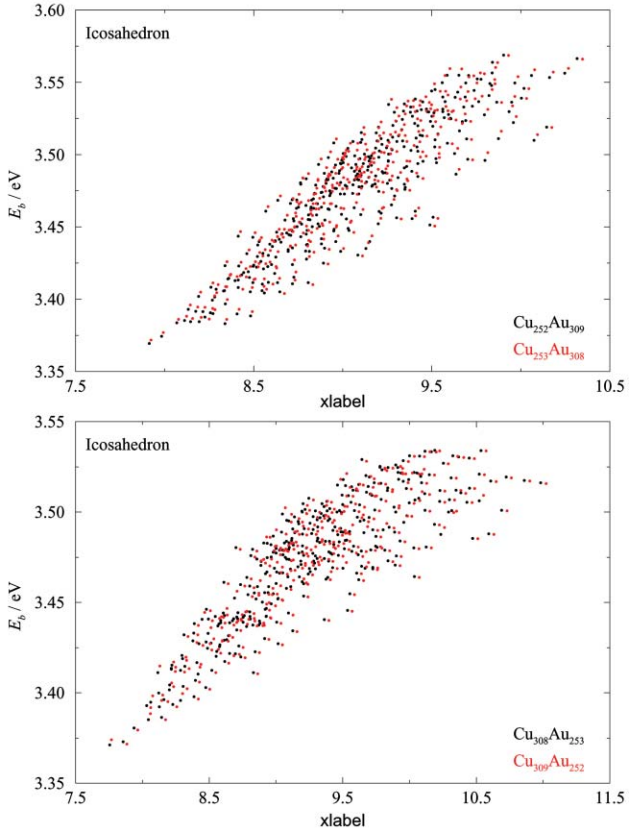

Fig. 5 Plot of binding energy (E_b) *vs.* the average distance of a gold atom from the cluster centre of mass ($\langle R_{Au} \rangle$) for all the homotops of four 561-atom Cu–Au icosahedral composomers.

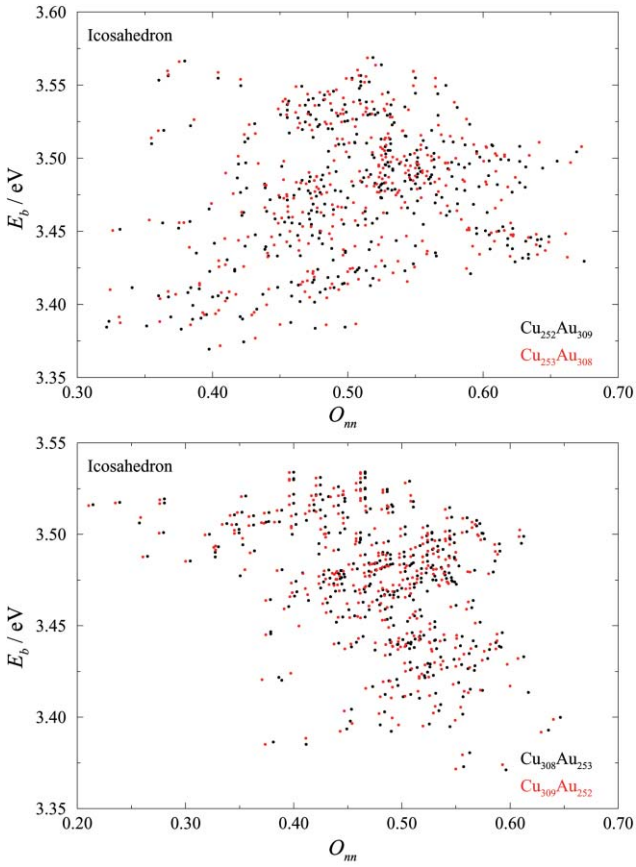

Fig. 6 Plot of binding energy (E_b) *vs.* the nearest-neighbour order parameter (O_{nn}) for all the homotops of four 561-atom Cu–Au icosahedral composomers.

are a number of homotops with high binding energies, which also have reasonably high O_{nn} values. This can be understood in terms of reduction of unfavourable interactions. In a bulk system, all the atoms have 12 nearest neighbours, so swapping atoms in a system with only a small mixing energy will produce only a small change in binding energy. For example, consider swapping a gold atom which has 12 gold nearest neighbours and a copper atom which has 12 copper nearest neighbours. This results in the loss of 12 Au–Au and 12 Cu–Cu interactions, and the creation of 24 Cu–Au interactions. As the mixing energy is weak, Cu–Au interactions are intermediate in strength between Au–Au and Cu–Cu (see Table 1), so the overall effect of the swap on the binding energy is small. Clusters, however, have atoms on the surface which have lower coordination numbers. Consider swapping a gold atom from the surface which has six gold nearest neighbours with a copper atom from the centre with 12 nearest neighbours. This results in the loss of 12 Cu–Cu interactions and only 6 Au–Au interactions and the creation of 18 Cu–Au interactions. As Cu–Au interactions are stronger than Cu–Cu, this has a stabilising effect on the energy. The situation is in fact more complex than this simple nearest-neighbour model suggests, as the bonding extends beyond nearest neighbours, but this provides a rationalisation for the stability trends in these mixed clusters.

3.2 Cuboctahedral nanoalloy clusters

The binding energies of all composomers and homotops for 1–4-shell cuboctahedral clusters are plotted in Fig. 7, with the same colour scheme as for Fig. 3. The clusters with gold at the surface (yellow and red points) are generally more stable than those with copper at the surface, as was observed for the icosahedral clusters. In contrast to the icosahedral clusters,

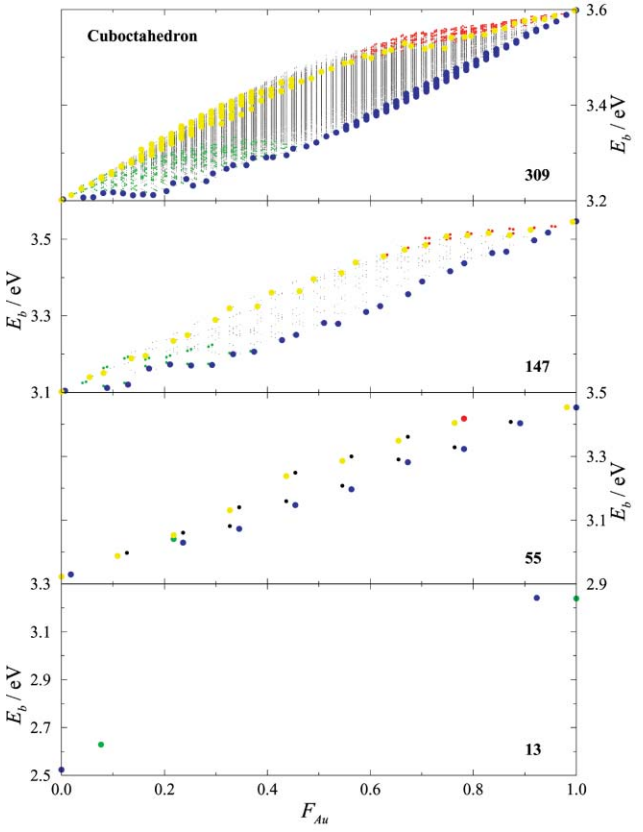

Fig. 7 Plot of binding energy (E_b) *vs.* the fraction of gold atoms (F_{Au}) for Cu_nAu_m cuboctahedral clusters, where $n + m$ is 13, 55, 147 and 309 atoms. Key: red = Au at surface; green = Cu at surface; blue = Cu surface and Au core; yellow = Au surface and Cu core.

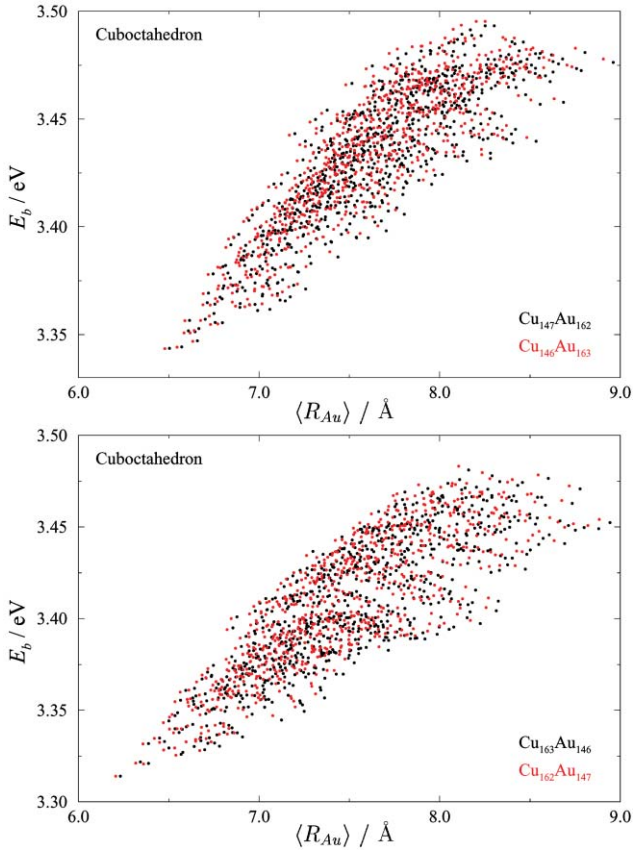

Fig. 8 Plot of binding energy (E_b) *vs.* the average distance of a gold atom from the cluster centre of mass ($\langle R_{Au} \rangle$) for all the homotops of four 309-atom Cu–Au cuboctahedral composomers.

however, for each nuclearity, the most stable clusters are those composed entirely of gold atoms (*i.e.* the highest E_b value is for $F_{Au} = 1$). This is due to the fact that there is no inherent strain in cuboctahedral clusters, so the introduction of copper atoms into a pure gold cluster leads to an increase in strain (by introducing a mismatch in the bond lengths), as well as introducing weaker Cu–Cu and Cu–Au interactions. At intermediate compositions ($F_{Au} \approx 0.5$) there is a slight increase in mixing (some black points with higher binding energies than the yellow points), which may be due to the fact that the absence of bulk strain is less of a driving force for Cu atoms to occupy core sites.

Fig. 8 and 9 show plots of the binding energy against $\langle R_A \rangle$ and O_{nn} for homotops of 4-shell cuboctahedral clusters with the compositions $Cu_{163}Au_{146}$, $Cu_{162}Au_{147}$, $Cu_{147}Au_{162}$ and $Cu_{146}Au_{163}$. (162 atoms are required to fill the outer shell of the 309-atom cuboctahedron.)

Fig. 8 shows that there is again a good correlation between E_b and $\langle R_{Au} \rangle$, confirming that clusters with gold on the surface are generally more stable. However, in contrast to the icosahedral clusters, the most stable homotops have slightly smaller values of $\langle R_{Au} \rangle$, suggesting that, for the most stable clusters, some gold atoms are closer to the centre of the cluster. Fig. 9 supports this conclusion, as some of the most stable homotops have relatively high values of O_{nn}, implying some mixing of the surface gold atoms into the core of the cluster.

3.3 Icosahedral *vs.* cuboctahedral cluster growth

In this study, we have found that, for the larger clusters, the icosahedral and cuboctahedral structures lie close in energy: for example, for 4-shell 309-atom clusters, the binding energies lie in the range 3.2–3.6 eV for both structure types, with the preferred geometrical structure type depending on the composition

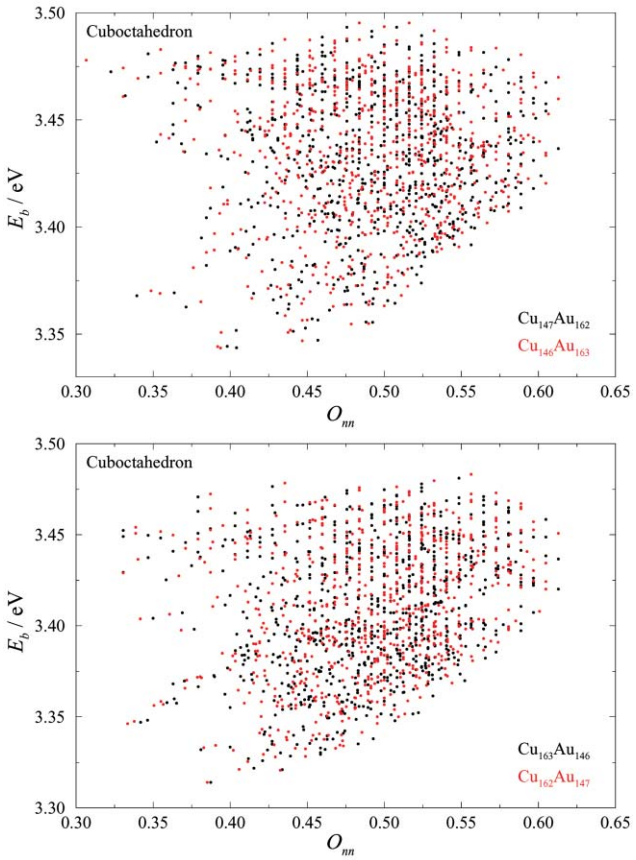

Fig. 9 Plot of binding energy (E_b) *vs.* the nearest-neighbour order parameter (O_{nn}) for all the homotops of four 309-atom Cu–Au cuboctahedral composomers.

and atom ordering. For the smaller clusters, however, the icosahedral clusters are generally more stable (possess higher binding energies) than the cuboctahedra. The predominance of icosahedral geometries for smaller nuclearities, which is due to the increased average coordination numbers and lower surface energies in these structures, is consistent with previous studies on elemental clusters, using empirical potentials (see, for example, ref. 28 and 29) and *ab initio* calculations (see, for example, ref. 44). In a recent genetic algorithm-based[45] study of Cu, Au and Cu–Au clusters with up to 56 atoms, we also found icosahedral clusters to be more stable than cuboctahedral ones.[38] As the clusters get larger, however, the increasing bulk strain inherent in the icosahedral geometry outweighs the lower surface energy and cuboctahedral (or other fcc-type) structures must eventually become more stable—the bulk CuAu, Cu_3Au and $CuAu_3$ alloys all have fcc structures[4] (if the atom ordering is ignored).

Interestingly, X-ray diffraction studies of thiol-passivated pure gold clusters indicate the presence of icosahedral and decahedral, as well as fcc-like metal cores.[46–48]

3.4 Comparison with results of full geometry optimisation for small Cu–Au clusters

In our previous study, we used a genetic algorithm to find the lowest energy structures (optimising both geometries and atom labelling) of pure Cu and Au clusters, and Cu–Au nanoalloys with up to 56 atoms and compositions corresponding to the Cu : Au ratios 3 : 1, 1 : 1 and 1 : 3.[38] In agreement with the results presented here, it was found that the lowest energy structures of Cu–Au nanoalloy clusters tend to have Cu atoms in the core and Au atoms on the surface. In the case of the 55-atom clusters, while Cu_{55} was found to adopt the 2-shell icosahedral structure, the lowest energy structure for Au_{55} has a low symmetry "amorphous structure",[38,49] though the replacement of a single Au atom by Cu is sufficient to make the icosahedral structure lowest in energy.[38] In the icosahedral $CuAu_{54}$ cluster, the Cu atom occupies the central site, which is again consistent with the findings presented here and with detailed studies of lower nuclearity clusters.[25]

The lowest energy structures found for $(CuAu)_M$ clusters are very similar to those of pure copper clusters in that they are predominantly based on the icosahedral structure. The degree of mixing in these clusters is quite small. The copper atoms group together in islands, *i.e.* they tend to form bonds with other copper atoms rather than gold atoms. As the clusters grow in size, the copper and gold atoms form shells within the clusters, with the central atom usually being a copper atom. As mentioned above, the smaller size of the central copper atom reduces the strain in icosahedral-type clusters.

The lowest energy structures found for $(Cu_3Au)_M$ and $(CuAu_3)_M$ clusters are again mainly based on icosahedral packing. The main difference between these two types of structure is that when the minority atom type is copper, layers of like atoms are formed (stabilising the cluster by maximising the number of strong Au–Au contacts), whereas when the gold atoms are in the minority, a more random (more mixed) arrangement of atoms is observed. This may be due to the fact that when gold is the minority atom, a greater gain in binding energy is obtained by dispersing the gold atoms throughout the cluster, thereby increasing the number of Cu–Au bonds and reducing the number of weaker Cu–Cu bonds. These results are in agreement with previous studies by López *et al.* on small Cu–Au clusters.[16]

3.5 Comparison of theory and experiment

In their original experiments on Cu–Au clusters, Mori and co-workers found that, when starting with 4 nm Au particles, the alloy clusters formed at room temperature are solid solutions (*i.e.* they are homogeneously mixed), while at lower temperatures, a two-phase structure results, with a Au core surrounded by a Cu–Au solid solution.[6,26] Independent of composition, solid solutions were found at temperatures well below the bulk order–disorder temperature (*e.g.* T_c = 663 K for bulk Cu_3Au[50]). For larger (10 nm) Au particles, Cu dissolution only occurs near the surface of the cluster, and for even larger (30 nm) particles, no dissolution occurs. In their study of stoichiometric $(Cu_3Au)_M$ clusters, Yasuda and Mori found that, for larger cluster sizes (9 and 20 nm), annealing results in ordering of the initially generated solid solutions, to give the $L1_2$ structure of bulk Cu_3Au.[27] For smaller clusters (4 nm), however, the solid solution is the most stable phase. In these studies, the local packing in the Cu–Au clusters was found to be fcc-like, as in the bulk alloy phases.

Pauwels, Lievens *et al.* have recently carried out electron diffraction and high resolution electron microscopy (HREM) studies of 1–4.5 nm Cu–Au clusters generated by laser vaporisation of bulk alloy targets followed by low energy deposition on amorphous carbon and MgO substrates.[8] It was found that the chemical compositions of the clusters match those of the target materials, with lattice spacings consistent with those of the bulk alloys. In the case of cluster deposition on amorphous carbon, a number of cluster morphologies were observed, such as cuboctahedra, decahedra (with 5-fold symmetry) and more spherical geometries with no clear morphology, often exhibiting twinning. For clusters deposited on MgO, however, only truncated octahedral morphologies were observed.

The electron diffraction and HREM experiments indicate that the stoichiometric $(CuAu)_M$, $(Cu_3Au)_M$ and $(CuAu_3)_M$ clusters all have fcc structures, *i.e.* the Cu and Au atoms are chemically disordered, forming a solid solution, both on amorphous carbon and MgO substrates.[8] These findings are consistent with the earlier results of Yasuda and Mori for the smaller Cu–Au particles.[27]

Pauwels, Lievens *et al.* also perfomed Monte Carlo (MC) simulations on free $(Cu_3Au)_M$ clusters,[8] using a potential (similar in nature to the Gupta potential) based on the second moment tight binding approximation.[51] The structures studied were isolated truncated octahedral clusters with 456 and 786 atoms and a "spherical" cluster of 959 atoms. The MC simulations predict that these clusters are not ordered (*i.e.* they do not have the $L1_2$ structure of ordered Cu_3Au throughout), but they are not completely homogeneous. In fact, the core is slightly deficient in Au and does exhibit $L1_2$ ordering, while the mantle is a Au-rich solid solution (the terms "Au-rich" and "Au-deficient" being relative to a homogeneous Cu_3Au distribution.) The core is predicted to be fully ordered at 300 K, undergoing a second order order–disorder transition at around 600 K.[8] These authors also found that substrate-induced strain (due to cluster–substrate lattice mismatch) can lead to the destruction of the core order.

Pauwels, Lievens *et al.* have presented a detailed discussion of possible reasons why their MC simulations disagree with the experimental results (both their own and those of Yasuda and Mori[27]), where there appears to be no evidence for core ordering and segregation of excess Au to the mantle.[8] It is pointed out that, experimentally, the Cu–Au clusters are not generated in thermodynamic equilibrium, being cooled rapidly by the He carrier gas, which may lead to the formation of metastable solid solutions. The process of cluster deposition, even at relatively low impact energies, may lead to cluster rearrangement and structural/ordering changes may be induced by interactions with the substrate (especially in the case of MgO). The sizes of the clusters are also relevant in that the MC simulations are generally performed on quite small clusters (with diameters of up to 3 or 4 nm) and many of the experiments have dealt with larger clusters (with diameters of upwards of 4 nm). Finally, the application of a potential energy

function, which was parameterised by fitting experimental properties of the bulk elements and alloys, to study finite alloy particles, is questioned.[8] In clusters, where there are a high proportion of surface atoms, the electronic structures of these atoms may be different from those in the bulk, rendering bulk-parameterised potentials of limited applicability.

Comparing our present results (which indicate a tendency towards segregation, with a Cu-rich core and Au-rich surface region) with the experimental results discussed above, these same factors can be invoked as possible reasons for differences. The largest clusters that we have studied (5-shell, 561-atom icosahedral clusters) again have diameters (2.88 nm) lower than those studied experimentally. The use of the Gupta potential (which was parameterised by fitting bulk properties) to study finite clusters, including clusters with compositions different from that of the alloy phase used in the parametrisation (Cu_3Au[33]) is again a source of concern.[38] In future work, we propose to include data obtained from electronic structure calculations (*e.g.* using density functional theory) on small clusters in the fitting of both the homo- and the heteronuclear parameters in the Gupta potential.

When comparing our results with the theoretical simulations of Pauwels, Lievens *et al.*,[8] it should be noted that they have considered truncated octahedral and "spherical clusters", while we have studied icosahedral and cuboctahedral geometries. Also, while they considered only clusters with the approximate composition Cu_3Au, we have looked at clusters ranging in composition from pure Cu to pure Au. As mentioned earlier, our subshell substitution approach means that we have only studied high symmetry structures, while the MC simulations can explore a wider variety of local ordered and disordered arrangements. Finally, our calculations are static energy calculations, performed at 0 K, so temperature effects have not been taken into account. At higher temperatures, entropy will, of course, favour random mixing over either segregation or ordering.

The closest direct comparion that can be made concerns Cu–Au nanoalloy clusters of composition Cu_3Au. In our previous calculations on $(Cu_3Au)_M$ clusters,[38] we noted a greater tendency towards Cu–Au mixing in these Au-deficient clusters than in the Au-rich or 50 : 50 mixtures, which is consistent with the predictions of Pauwels, Lievens *et al.* The similarity in the types of potentials used in these studies, and the fact that both were parameterised by fitting bulk properties, leads us to conclude that similar results should be obtained if analogous calculations were performed, though any comparison with experiment is limited by the factors mentioned above.

4 Conclusions

Energy calculations (with radial relaxion) have been carried out on icosahedral and cuboctahedral Cu–Au nanoalloy clusters, of varying composition, within the constraints that the atoms in each subshell are either all Cu or all Au, with the interatomic interactions modelled by the Gupta many-body potential. It was found that for each composition, the lowest energy homotops tend to have predominantly Au atoms on the surface and Cu atoms in the core, which may be explained in terms of the lower surface energy of Au compared to Cu. More detailed considerations of mixing and segregation have also taken into account the relative strength of Cu–Cu, Cu–Au and Au–Au bonding interactions and, in the case of icosahedral clusters, the relief of bulk strain that is possible upon substituting the smaller Cu atoms for Au in the compressed core. Further studies are currently underway to ascertain the relative importance of these effects in different types of intermetallic clusters.

A number of order parameters and mixing energies have been introduced and it has been shown that, while there is generally little correlation between the cluster binding energy and the nearest-neighbour ordering (as measured by O_{nn}), there is good correlation with the average distance of the Au atoms from the centre of the cluster ($\langle R_{Au} \rangle$). A similar correlation, of increasing binding energy with increasing average radial distance of one type of atom, has previously been observed by Montejano-Carrizales *et al.* for Cu–Ni nanoalloys, where the most stable clusters have Cu atoms on the surface.[52] For the largest icosahedral clusters studied (with 561 atoms), the plot of mixing energy (ΔE_{mix}) against composition is fairly smooth, peaking at the 50 : 50 mixture. More detailed studies of the correlation of cluster stability with various ordering parameters and mixing energies will be undertaken in the future.

Comparisons have been made with previous theoretical calculations on Cu–Au clusters, as well as with experimental studies of the structures and atom ordering of deposited Cu–Au particles. Our results have been shown to be consistent with previous calculations and possible reasons for certain disagreements with experimental results have been discussed. Future studies will focus on the inclusion of data on small elemental and bimetallic clusters in the parameterisation of empirical potentials for modelling nanoalloys.

Acknowledgements

The authors wish to thank Professor Julius Jellinek, Dr Alvaro Posada-Amarillas and Mr Mark Bailey for helpful discussions. N. T. W. is grateful to EPSRC for a Ph.D. studentship.

References

1 R. L. Johnston, *Atomic and Molecular Clusters*, Taylor and Francis, London, 2002.
2 J. Jortner, *Z. Phys. D*, 1992, **24**, 247.
3 R. L. Johnston, *Philos. Trans. R. Soc. London, Ser. A*, 1998, **356**, 211.
4 W. B. Pearson, *The Crystal Chemistry and Physics of Metals and Alloys*, Wiley, New York, 1972.
5 S. Giorgio, H. Graoui, C. Chapan and C. R. Henry, in *Metal Clusters in Chemistry*, ed. P. Braunstein, L. A. Oro and P. R. Raithby, Wiley-VCH, Weinheim, 1999, vol. 2, p. 1194.
6 H. Mori, M. Komatsu, K. Takeda and H. Fujita, *Philos. Mag. Lett.*, 1991, **63**, 173.
7 W. Biuwen, F. Vanhoutte, F. Despa, S. Bouckaert, S. Neukermans, L. T. Kuhn, H. Weidele, P. Lievens and R. E. Silverans, *Chem. Phys. Lett.*, 1999, **314**, 227.
8 B. Pauwels, G. Van Tendeloo, E. Zhurkin, M. Hou, G. Verschoren, L. Theil Kuhn, W. Bouwen and P. Lievens, *Phys. Rev. B*, 2001, **63**, 165406.
9 J. Jellinek and E. B. Krissinel, in *Theory of Atomic and Molecular Clusters*, ed. J. Jellinek, Springer, Berlin, 1999, pp. 277–308, and references therein.
10 A. V. Ruban, H. L. Skriver and J. K. Nørskov, *Phys. Rev. B*, 1999, **59**, 15990.
11 A. M. Molenbroek, S. Haukka and B. S. Clausen, *J. Phys. Chem. B*, 1998, **102**, 10680.
12 G. Schmid, in *Metal Clusters in Chemistry*, ed. P. Braunstein, L. A. Oro and P. R. Raithby, Wiley-VCH, Weinheim, 1999, vol. 3, p. 1325.
13 M. P. Andrews and S. C. O'Brien, *J. Phys. Chem.*, 1992, **96**, 8233.
14 *Atomistic Simulation of Materials: Beyond Pair Potentials*, ed. V. Vitek and D. J. Srolovitz, Plenum, New York, 1989.
15 A. Christensen, P. Stolze and J. K. Nørskov, *J. Phys. Condens. Matter*, 1995, **7**, 1047.
16 M. J. López, P. A. Marcos and J. A. Alonso, *J. Chem. Phys.*, 1996, **104**, 1056.
17 J. Jellinek and E. B. Krissinel, *Chem. Phys. Lett.*, 1996, **258**, 283.
18 E. B. Krissinel and J. Jellinek, *Chem. Phys. Lett.*, 1997, **272**, 301.
19 E. B. Krissinel and J. Jellinek, *Int. J. Quantum Chem.*, 1997, **62**, 185.
20 J. Jellinek and M. J. López, *J. Chem. Phys.*, 1999, **110**, 8899.
21 A. Fortunelli and A. M. Velasco, *J. Mol. Struct. (THEOCHEM)*, 1999, **487**, 251.
22 S. Bromley, G. Sankar, C. R. A. Catlow, T. Maschmeyer, B. F. G. Johnson and J. M. Thomas, *Chem. Phys. Lett.*, 2001, **340**, 524.

23 G. Pacchioni, S.-C. Chung, S. Krüger and N. Rösch, *Chem. Phys.*, 1994, **184**, 125.
24 B. Hartke, *Theor. Chem. Acc.*, 1998, **99**, 241.
25 R. A. Lordeiro, F. F. Guimarães, J. C. Belchior and R. L. Johnston, *Phys. Chem. Chem. Phys.*, submitted.
26 H. Yasuda and H. Mori, *Z. Phys. D*, 1994, **31**, 131.
27 H. Yasuda and H. Mori, *Z. Phys. D*, 1996, **37**, 181.
28 J. E. Hearn and R. L. Johnston, *J. Chem. Phys.*, 1997, **107**, 4674.
29 G. W. Turner, R. L. Johnston and N. T. Wilson, *J. Chem. Phys.*, 2000, **112**, 4773.
30 N. A. Besley, R. L. Johnston, A. J. Stace and J. Uppenbrink, *J. Mol. Struct. (THEOCHEM)*, 1995, **341**, 75.
31 N. T. Wilson, *The Structure and Dynamics of Noble Metal Clusters*, Ph.D. Thesis, University of Birmingham, UK, 2000.
32 M. S. Bailey, *A Theoretical Investigation of Nano-Alloy Clusters*, M. Nat. Sci. 4th Year Project Report, University of Birmingham, UK, 2000.
33 F. Cleri and V. Rosato, *Phys. Rev. B*, 1993, **48**, 22.
34 R. P. Gupta, *Phys. Rev. B*, 1981, **23**, 6265.
35 R. R. Hultgren, P. D. Desai, D. T. Hawkins, M. Gleiser and K. K. Kelley, *Selected Values of the Thermodynamic Properties of Binary Alloys*, American Soc. Metals, Materials Park, OH, USA, 1973.
36 C. Kittel, *Introduction to Solid State Physics*, John Wiley, New York, 6th edn., 1986.
37 *NAG Fortran Library*, version 16, Numerical Algorithms Group, Oxford, 1993.
38 S. Darby, T. V. Mortimer-Jones, R. L. Johnston and C. Roberts, *J. Chem. Phys.*, 2002, **116**, 1536.
39 O. J. Lanning, *Theoretical Study of Structures and Properties of Alloys*, M. Nat. Sci. 4th Year Project Report, University of Birmingham, UK, 2001.
40 J. Xie, J. A. Northby, D. L. Freeman and J. D. Doll, *J. Chem. Phys.*, 1989, **91**, 612.
41 J. P. K. Doye and D. J. Wales, *J. Phys. B*, 1996, **29**, 4859.
42 A. R. Miedema, *Z. Metallkd.*, 1978, **69**, 287.
43 H. Cox, X. Liu and J. N. Murrell, *Mol. Phys.*, 1998, **93**, 921.
44 G. Pacchioni and J. Koutecky, *J. Chem. Phys.*, 1984, **81**, 3588.
45 C. Roberts, R. L. Johnston and N. T. Wilson, *Theor. Chem. Acc.*, 2000, **104**, 123.
46 C. L. Cleveland, U. Landman, M. N. Shafigullin, P. W. Stephens and R. L. Whetten, *Z. Phys. D*, 1997, **40**, 503.
47 R. L. Whetten, M. N. Shafigullin, J. T. Khoury, T. G. Schaaff, I. Vezmar, M. M. Alvarez and A. Wilkinson, *Acc. Chem. Res.*, 1999, **32**, 397.
48 D. Zanchet, B. D. Hall and D. Ugarte, *J. Phys. Chem. B*, 2000, **104**, 11013.
49 J. M. Soler, M. R. Beltrán, K. Michaelian, I. L. Garzón, P. Ordejón, D. Sánchez-Portal and E. Artacho, *Phys. Rev. B*, 2000, **61**, 5771.
50 M. Hansen and K. Anderko, *Constitution of Binary Alloys*, McGraw Hill, New York, 2nd edn., 1958.
51 G. J. Ackland and V. Vitek, *Phys. Rev. B*, 1990, **41**, 10324.
52 J. M. Montejano-Carrizales, M. P. Iñiguez and J. A. Alonso, *Phys. Rev. B*, 1994, **49**, 16649.